Resonance behavior of atomic and molecular photoionization amplitudes

N. A. Cherepkov,* V. V. Kuznetsov, and S. K. Semenov
State University of Aerospace Instrumentation, Bol'shaya Morskaya 67, 190000 St. Petersburg, Russia
(Received 20 April 2007; published 20 July 2007)

The behavior of the partial photoionization amplitudes with a given orbital angular momentum l in the complex plane in resonances is studied. In the autoionization resonances the trajectory of the amplitude in the complex plane corresponds to a circle. With increasing photoelectron energy the amplitude moves about a circle in the counterclockwise direction. The new expressions for the partial amplitudes in the resonance are proposed which are similar to the Fano form but contain the "partial" profile parameters which are connected with the Fano parameter q by a simple relation. In the giant dipole resonances the amplitudes in the complex plane also move about a circle in the counterclockwise direction provided the Coulomb phase is excluded from the amplitude. In the correlational resonances created by channel interactions with the giant dipole resonance the trajectories of the amplitudes acquire a loop about which the amplitudes move in the counterclockwise direction. Very similar behavior of partial photoionization amplitudes in the complex plane is demonstrated also for the dipole transitions from the K shells of the N_2 molecule in the σ^* shape resonance.

DOI: 10.1103/PhysRevA.76.012715 PACS number(s): 33.80.Eh, 32.80.Fb

I. INTRODUCTION

Resonances are common features of all quantum processes, therefore it is of great importance to study their general properties. From elastic scattering of particles on different targets it is well known that the resonance structures are described by the Breit-Wigner amplitude [1,2]. The Argand diagram of this amplitude in the complex plane gives a circle [3]. When the particle energy varies from 0 to infinity, the Breit-Wigner amplitude moves in a complex plane about a circle in the counterclockwise direction. There were many studies of scattering amplitudes for different projectiles and targets (see Refs. [3–6], and references therein). We would like to perform the analogous study of photoionization amplitudes. It used to be said that photoionization is a half-scattering process since the continuous spectrum wave function enters the amplitude only once in the final state. But that is sufficient for the photoionization amplitudes to have resonance properties similar to the properties of the electron scattering amplitudes. During the last decades starting from the pioneering work of Fano [7] much attention was given to the studies of autoionization resonances in atoms [8–14], though usually they were concentrated on the description of the photoionization cross section.

The knowledge of the behavior of complex photoionization amplitudes is important and helpful in many cases, and in particular, in performing the complete experiments which became now feasible both for atoms [15–18] and molecules [15,18–21]. The complete, or perfect, experiment means an experiment from which one can extract all quantum-mechanical amplitudes necessary for a theoretical description of the process [22,23]. Since every theoretical description is valid within some approximation, the concept of the complete experiment is valid within the same approximation, too. Up to now the complete photoionization experiments with atoms and molecules were restricted by the electric dipole approximation accepted in this paper. In many cases the complete experiment does not give a unique solution [19–21], and the knowledge of the general behavior of amplitudes in the complex plane can be helpful in removing ambiguities [19].

Another use of complex amplitudes is connected with the studies of the angular distribution and spin polarization of photoelectrons [24], or polarization state of residual ions in resonances. One way is to look for parametrization of these characteristics in the autoionization resonances through the Fano parameters [7,8] introduced for the description of the total photoionization cross section, as was proposed in Refs. [11,25]. An alternative way is to insert the resonance photoionization amplitudes introduced in this paper into the well known equations for these parameters derived without taking the resonances into account [24].

And finally, presentation of amplitudes as an Argand plot in the complex plane gives a convenient visualization of their resonance properties and helps to better understand the character of electron interactions in atoms and molecules. The dipole amplitudes in autoionization resonances at best illustrate the resonance properties of the amplitudes in the complex plane. Therefore we start our consideration from the example of the $3p$ autoionization resonance in Ne. After that we demonstrate that the famous giant dipole resonance in photoionization of the $4d$ shell of Xe is the resonance of the Breit-Wigner type which already exists in different single particle approximations. As the next step, we show that the correlational interaction between any open transition and the giant dipole resonance leads to appearance of a maximum in that transitions which is represented by a loop in the Argand plot of the corresponding amplitude. And finally, we analyze the behavior on the complex plane of all dipole amplitudes with $0 \leqslant l \leqslant 5$ from the K shells of N_2 molecule in the σ^* shape resonance.

II. BREIT-WIGNER AMPLITUDE

Before starting the consideration of photoionization amplitudes we would like to remind the reader of well known

*nik_cherepkov@yahoo.com

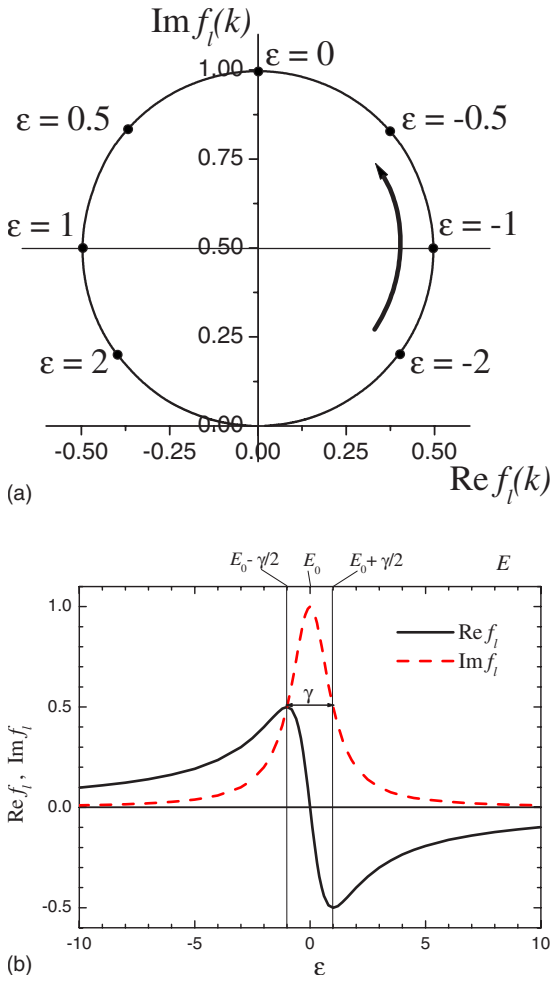

FIG. 1. (Color online) (a) The Argand plot of the Breit-Wigner amplitude (1). (b) The real and imaginary parts of the Breit-Wigner amplitude (1).

properties of the scattering amplitude. Suppose that there is a quasistationary state with the orbital angular momentum l in the electron scattering on some target. Then the partial resonance amplitude $f_l(k)$ corresponding to the elastic scattering without a background is presented by the Breit-Wigner equation [1–3]

$$f_l(k) = \frac{\gamma/2}{E_0 - E - i\gamma/2} = -\frac{1}{\varepsilon + i} = \frac{i - \varepsilon}{\varepsilon^2 + 1}, \tag{1}$$

where

$$\varepsilon = (E - E_0)/(\gamma/2), \tag{2}$$

$E=k^2/2$ is the electron energy (atomic units $\hbar=m=e=1$ are used in this paper), E_0 is the resonance energy, and γ is the resonance width. The Argand diagram of this amplitude in the complex plane $x=\mathrm{Re}\, f_l(k)$, $y=\mathrm{Im}\, f_l(k)$, is presented in Fig. 1(a). It corresponds to a circle which goes through the origin and has its center on the y axis. When the electron energy E varies from 0 to infinity, the Breit-Wigner amplitude moves about a circle in the counterclockwise direction. At $E=0$ the phase of the amplitude is close to zero, and with increasing energy the phase increases by π. There are some characteristic points on this circle, namely, (i) the points $\varepsilon=0$ and $\varepsilon=\pm\infty$ are on the vertical diameter of the circle and (ii) the points $\varepsilon=\pm 1$ are on the horizontal diameter of the circle, and they define the width γ of the resonance because $E-E_0=-\gamma/2$ at $\varepsilon=-1$, and $E-E_0=\gamma/2$ at $\varepsilon=+1$ [see Fig. 1(b)]. One can say that the points $\varepsilon=0$ and $\varepsilon=\pm\infty$, on one side, and $\varepsilon=\pm 1$, on the other side, are situated on the mutually perpendicular diameters of the circle. This property will be used later for the graphical definition of E_0 and γ of photoionization amplitudes. In Fig. 1(b) we show separately $\mathrm{Re}\, f_l(k)$ and $\mathrm{Im}\, f_l(k)$ as functions of the variable ε.

III. AUTOIONIZATION RESONANCES

A. Random phase approximation

Let us consider now the autoionization resonances which appear before the second and all higher ionization thresholds of atoms and molecules when a discrete excitation of a deeper shell interacts with one or several ionization continua of the shell(s) with lower ionization potential. In the case of atoms the photoionization cross section is expressed as usual [26]

$$\sigma_{nl}(\omega) = \frac{4\pi^2 \alpha \omega N_{nl}}{3(2l+1)} \sum_{l_1} |\langle El_1 \| d \| nl \rangle|^2, \tag{3}$$

where α is the fine-structure constant, ω is the photon energy, $\omega=I_{nl}+E$, E is the photoelectron energy, I_{nl} and N_{nl} are the ionization potential and the number of electrons of the nl shell, and $\langle El_1 \| d \| nl \rangle$ is the reduced dipole matrix element in a single particle approximation. The consideration in this paper is restricted by the nonrelativistic approximation in which there are two dipole allowed transitions from the nl shell, namely, $nl \to E, l+1$, and $nl \to E, l-1$. We will also imply for simplicity that the closed shell atoms are ionized so that $N_{nl}=2(2l+1)$. In a single particle approximation the reduced dipole matrix element is

$$\langle El_1 \| d \| nl \rangle = \hat{l}\hat{l}_1 (-1)^l \begin{pmatrix} l & 1 & l_1 \\ 0 & 0 & 0 \end{pmatrix} \int_0^\infty R_{nl}(r) R_{El_1}(r) r^3 dr, \tag{4}$$

where $\hat{l} \equiv \sqrt{2l+1}$, $R_{nl}(r)$ and $R_{El_1}(r)$ are (real) single particle wave functions of an electron in the initial and final states, respectively. The matrix element (4) is real. As a rule the Hartree-Fock (HF) approximation is used nowadays as a single particle approximation. All other physical quantities like the angular asymmetry parameter β [26], the spin polarization parameters [24] are expressed through these reduced dipole matrix elements.

In single particle approximations the autoionization resonances do not appear, therefore it is necessary to take into account the interaction between the discrete excited state and the photoionization continuum in some approximation. In particular, one can apply the random phase approximation with exchange (RPAE) [27] which is frequently used in photoionization calculations. The dipole matrix element in the RPAE is defined by the equation

$$\langle El_1\|D(\omega)\|nl\rangle = \langle El_1\|d\|nl\rangle + \sum_{\substack{E_2,l_2>F \\ n',l'\leqslant F}} \left[\frac{\langle E_2l_2\|D(\omega)\|n'l'\rangle\langle n'l',El_1\|U_1\|E_2l_2,nl\rangle}{3(\omega - E_2 + E_{n'l'} + i\delta)} - \frac{\langle n'l'\|D(\omega)\|E_2l_2\rangle\langle E_2l_2,El_1\|U_1\|n'l',nl\rangle}{3(\omega + E_2 - E_{n'l'} - i\delta)} \right], \tag{5}$$

where in the denominators $\delta \to +0$, $\langle n'l', El_1\|U_L\|E_2l_2, nl\rangle$ are the reduced Coulomb matrix elements

$$\langle n'l', El_1\|U_L\|E_2l_2, nl\rangle = 2\langle n'l', El_1\|V_L\|E_2l_2, nl\rangle - \hat{L}^2 \sum_{L'=0}^{\infty} (-1)^{L+L'} \begin{Bmatrix} l' & L & l_2 \\ l_1 & L' & l \end{Bmatrix} \times \langle n'l', El_1\|V_{L'}\|nl, E_2l_2\rangle, \tag{6}$$

and

$$\langle n'l', El_1\|V_L\|E_2l_2, nl\rangle = \int\int R^*_{n'l'}(r) R^*_{El_1}(r') \frac{r_<^L}{r_>^{L+1}} \times R_{E_2l_2}(r) R_{nl}(r') dr dr'. \tag{7}$$

As a result of the RPAE calculation for ionization of a given nl subshell we obtain the amplitudes $\langle El_1\|D(\omega)\|nl\rangle$ for two dipole allowed transitions $nl \to E, l+1$, and $nl \to E, l-1$, which interact with the resonance transition from another shell, say, with $n'l' \to n_s l_s$. To simplify the notations in Eq. (5) we will denote below the transitions by only one letter, namely, $nl \to El_1 \Rightarrow \mu$, $n'l' \to E_2l_2 \Rightarrow \nu$, $n'l' \to n_s l_s \Rightarrow s$. Then Eq. (5) is transformed to

$$D_\mu(\omega) = d_\mu + \frac{1}{3}\sum_\nu \left[\frac{D_\nu(\omega) U_{\nu\mu}}{\omega - \omega_\nu + i\delta} - \frac{D_{\tilde{\nu}}(\omega) U_{\tilde{\nu}\mu}}{\omega + \omega_\nu - i\delta} \right], \tag{8}$$

where the summation over ν means the summation over all one particle-one hole excitations of the system. It is useful to write this equation in another form through the so-called effective interaction Γ

$$D_\mu(\omega) = d_\mu + \frac{1}{3}\sum_\nu \left[\frac{d_\nu \Gamma_{\nu\mu}(\omega)}{\omega - \omega_\nu + i\delta} - \frac{d_{\tilde{\nu}} \Gamma_{\tilde{\nu}\mu}(\omega)}{\omega + \omega_\nu - i\delta} \right] \tag{9}$$

defined by an equation similar to Eq. (8)

$$\Gamma_{\mu\tau}(\omega) = U_{\mu\tau} + \frac{1}{3}\sum_\nu \left[\frac{U_{\mu\nu}\Gamma_{\nu\tau}(\omega)}{\omega - \omega_\nu + i\delta} - \frac{U_{\mu\tilde{\nu}}\Gamma_{\tilde{\nu}\tau}(\omega)}{\omega + \omega_\nu - i\delta} \right]. \tag{10}$$

When the photon energy ω tends to the energy of the discrete excitation in the single-particle approximation ω_s, $\omega_s = E_{n_s l_s} - E_{n'l'}$, the first term in square brackets of Eqs. (5) and (8)–(10) tends to infinity. Therefore we divide the amplitude D_μ as well as the effective interaction $\Gamma_{\mu\tau}$ into two parts. The nonresonant parts $D^0_\mu(\omega)$ and $\Gamma^0_{\mu\tau}(\omega)$ are the solutions of Eqs. (9) and (10), respectively, where the contribution of the divergent term (that is the term with $\nu = s$) is excluded. After that the remaining divergent terms are summed separately in the following way (below we omit for simplicity the argument ω in the amplitudes):

$$D_\mu = D^0_\mu + D^0_s \frac{\Gamma^0_{s\mu}}{3(\omega - \omega_s)} + D^0_s \frac{\Gamma^0_{ss}}{3(\omega - \omega_s)} \frac{\Gamma^0_{s\mu}}{3(\omega - \omega_s)} + \cdots = D^0_\mu + D^0_s \left[1 + \frac{\Gamma^0_{ss}}{3(\omega - \omega_s)} + \left(\frac{\Gamma^0_{ss}}{3(\omega - \omega_s)} \right)^2 + \cdots \right] \times \frac{\Gamma^0_{s\mu}}{3(\omega - \omega_s)}. \tag{11}$$

This equation is easily solved algebraically [10]

$$D_\mu = D^0_\mu + \frac{D^0_s \Gamma^0_{s\mu}}{3(\omega - \omega_s - \Gamma^0_{ss}/3)} = D^0_\mu \left[1 - \frac{D^0_s \Gamma^0_{s\mu}}{(\varepsilon + i) D^0_\mu \operatorname{Im} \Gamma^0_{ss}} \right], \tag{12}$$

where

$$\varepsilon = \frac{\omega - \omega_s - \operatorname{Re} \Gamma^0_{ss}/3}{-\operatorname{Im} \Gamma^0_{ss}/3} = \frac{\omega - \omega_0}{\gamma/2}. \tag{13}$$

ω_0 is the excitation energy with the correlational corrections included

$$\omega_0 = E_{n_s l_s} - E_{n'l'} + \operatorname{Re} \Gamma^0_{ss}/3 \tag{14}$$

and γ is the resonance width

$$\gamma = -2 \operatorname{Im} \Gamma^0_{ss}/3. \tag{15}$$

If the resonance is sufficiently narrow, all the values in Eqs. (12)–(15) except for ε can be implied to be constant within the resonance width. Though we derived Eq. (12) within the RPAE approximation it has much broader applicability.

Equation (12) for the photoionization amplitude can be compared with Eq. (25) of Starace [12]

$$D_\mu = D^0_\mu \left[1 + \alpha^*_\mu \frac{q - i}{\varepsilon + i} \right]. \tag{16}$$

Here q is the Fano parameter which is discussed in detail below, and a_μ is a complex parameter. It is implied that in the narrow energy region of a resonance the parameters D^0_μ, q, and a_μ are constants, and entire energy dependence of the dipole matrix element comes from the reduced energy variable ε. Equation (16) is a complex conjugate of the corresponding Eq. (25) of Ref. [12] where the complex conjugate matrix element $\langle nl\|D(\omega)\|\mu\rangle$ is treated instead of $\langle \mu\|D(\omega)\|nl\rangle$ accepted in this paper. Equations (12) and (16) have the same dependence on the energy variable ε, and they differ by the fact that Eq. (16) contains the Fano parameter q which is absent from Eq. (12).

B. Graphical presentation of the photoionization amplitudes

Let us present the amplitude (12) in the following form:

$$D_\mu = D_\mu^0\left[1 + \frac{C_{1\mu} + iC_{2\mu}}{\varepsilon + i}\right] = \frac{D_\mu^0}{\varepsilon + i}\left[\varepsilon + C_{1\mu} + i(1 + C_{2\mu})\right], \tag{17}$$

where $C_{1\mu}$ and $C_{2\mu}$ are real parameters constant within the resonance. This is a linear fractional transformation which maps the real axis of the variable ε onto the circle in the complex plane of D_μ. As a result, the Argand plot of this amplitude (in which the x and y axes correspond to $\mathrm{Re}\, D_\mu$ and $\mathrm{Im}\, D_\mu$, respectively) is a circle with the coordinates of the center defined by the equations

$$x_{0\mu} = \frac{1}{2}[(2 + C_{2\mu})\mathrm{Re}\, D_\mu^0 + C_{1\mu}\, \mathrm{Im}\, D_\mu^0],$$

$$y_{0\mu} = \frac{1}{2}[(2 + C_{2\mu})\mathrm{Im}\, D_\mu^0 - C_{1\mu}\, \mathrm{Re}\, D_\mu^0], \tag{18}$$

and of the radius

$$R_\mu = \frac{1}{2}\sqrt{|D_\mu^0|^2(C_{1\mu}^2 + C_{2\mu}^2)}. \tag{19}$$

In Fig. 2 we show the Argand plot of the dipole amplitudes D_s and D_d corresponding to two transitions $2p \to Es$ and $2p \to Ed$, respectively, in the $2s \to 3p$ autoionization resonance of Ne atom calculated in the RPAE approximation [27]. The number of energy points in the resonance is rather large in order to clearly draw the trajectory of the amplitude. Some energy points are marked in Fig. 2. In both cases we see the circles. When the photoelectron energy E is increasing the amplitudes D_s and D_d move counterclockwise about the circles. From the Argand plot we can find geometrically the resonance energy ω_0 and the width γ by analogy with the Breit-Wigner case. To this end we first mark the point on the circle which corresponds to $|\varepsilon| \to \infty$. In this limit according to Eq. (17) $D_\mu \to D_\mu^0$ [in Fig. 2(a) we show also the amplitude D_d outside the resonance in order to better define the limit $|\varepsilon| \to \infty$]. Then we draw the diameter through this point, and the opposite end of the diameter corresponds to $\varepsilon = 0$, that is to $\omega = \omega_0$. As the next step we draw another diameter perpendicular to the first one, and the second diameter crosses the circle at the points corresponding to $\varepsilon = \pm 1$ and $\omega - \omega_0 = \pm\gamma/2$ [see Fig. 1(b)].

To describe analytically the contour of the autoionization resonance calculated numerically in the RPAE, we fit the amplitudes D_μ using slightly different parametrization

$$\mathrm{Re}\, D_\mu = \mathrm{Re}\, D_\mu^0 + \frac{a_\mu \varepsilon + b_\mu}{\varepsilon^2 + 1}, \quad \mathrm{Im}\, D_\mu = \mathrm{Im}\, D_\mu^0 + \frac{b_\mu \varepsilon - a_\mu}{\varepsilon^2 + 1}. \tag{20}$$

Here a_μ, b_μ are real parameters which can be easily expressed through the parameters $C_{1\mu}$, $C_{2\mu}$

$$a_\mu = C_{1\mu}\, \mathrm{Re}\, D_\mu^0 - C_{2\mu}\, \mathrm{Im}\, D_\mu^0, \tag{21}$$

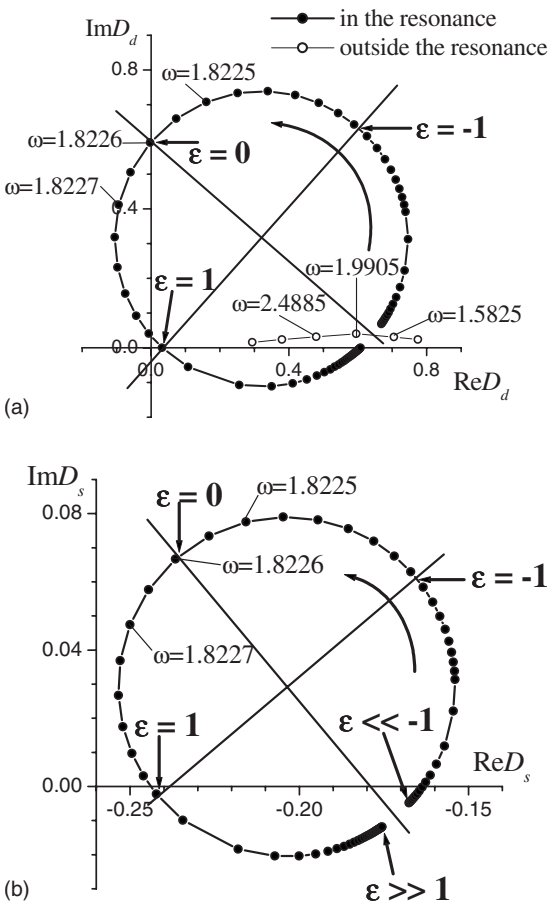

FIG. 2. The Argand plot of the amplitudes of the $2p \to Ed$ (a) and $2p \to Es$ (b) transitions of Ne atom calculated in the RPAE approximation in the region of the $2s \to 3p$ autoionization resonance.

$$b_\mu = C_{2\mu}\, \mathrm{Re}\, D_\mu^0 + C_{1\mu}\, \mathrm{Im}\, D_\mu^0. \tag{22}$$

Evidently, the parameters $C_{1\mu}$, $C_{2\mu}$ and a_μ, b_μ are equivalent. The parameters $C_{1\mu}$, $C_{2\mu}$ are convenient for describing the position of the circle on the complex plane, while the parameters a_μ, b_μ are convenient in fitting the real and imaginary parts of the amplitudes. The cross section for a particular transition is defined through these parameters by the equation

$$\begin{aligned}\sigma_\mu(\omega) &= \frac{4\pi^2 \alpha \omega N_{nl}}{3(2l+1)}|\mathrm{Re}\, D_\mu + i\, \mathrm{Im}\, D_\mu|^2 \\ &= \frac{\sigma_\mu^0(\omega)}{(1+\varepsilon^2)}\left\{\varepsilon^2 + 2\varepsilon\frac{a_\mu\, \mathrm{Re}\, D_\mu^0 + b_\mu\, \mathrm{Im}\, D_\mu^0}{|D_\mu^0|^2} + \frac{(a_\mu - \mathrm{Im}\, D_\mu^0)^2 + (b_\mu + \mathrm{Re}\, D_\mu^0)^2}{|D_\mu^0|^2}\right\},\end{aligned} \tag{23}$$

which can be rewritten in a more compact and more traditional form

$$\sigma_\mu = \frac{\sigma_\mu^0(\omega)}{1+\varepsilon^2}[(q_\mu+\varepsilon)^2 + t_\mu], \tag{24}$$

where

$$\sigma_\mu^0(\omega) = \frac{4\pi^2\alpha\omega N_{nl}}{3(2l+1)}|D_\mu^0|^2, \tag{25}$$

$$q_\mu = \frac{a_\mu \,\mathrm{Re}\, D_\mu^0 + b_\mu \,\mathrm{Im}\, D_\mu^0}{|D_\mu^0|^2} = C_{1\mu}, \tag{26}$$

and

$$t_\mu = \frac{(a_\mu - \mathrm{Im}\, D_\mu^0)^2 + (b_\mu + \mathrm{Re}\, D_\mu^0)^2}{|D_\mu^0|^2} - q_\mu^2 = (1+C_{2\mu})^2. \tag{27}$$

The parameter q_μ in the partial cross section (24) plays the same role as the Fano parameter q plays in the total cross section. The total cross section is the sum of the partial cross sections (24)

$$\sigma(\omega) = \sum_\mu \sigma_\mu(\omega) = \sum_\mu \frac{\sigma_\mu^0(\omega)}{(1+\varepsilon^2)}[(q_\mu+\varepsilon)^2 + t_\mu]. \tag{28}$$

We can compare it with the Fano equation for the total cross section in the resonance [8]

$$\sigma = \sigma_b + \sigma_a \frac{(q+\varepsilon)^2}{1+\varepsilon^2} = \sigma_0\left[1 - \rho^2 + \rho^2\frac{(q+\varepsilon)^2}{1+\varepsilon^2}\right], \tag{29}$$

where q is the Fano parameter defining the shape of the autoionization resonance in the total cross section, and

$$\rho^2 = \frac{\sigma_a}{\sigma_a+\sigma_b} \tag{30}$$

σ_a and σ_b are the parts of the cross section interacting and noninteracting with the resonance, respectively, and $\sigma_0 = \sigma_a + \sigma_b$. It is implied that within the resonance the cross sections σ_a and σ_b are constant. In practice usually both photoionization channels characterized by definite values of the orbital angular momentum l are interacting with the resonance. This is the case in particular for the $3p$ resonance in Ne considered in this paper. Both ionization channels, $2p \to Es$ and $2p \to Ed$, interact with the resonance, and we must form a linear combination of these channels in order to define the cross sections σ_a and σ_b. But we prefer to continue consideration within the partial wave channels.

We can present the cross section (29) as

$$\sigma = \sigma_0 \frac{\varepsilon^2 + \varepsilon r + s}{1+\varepsilon^2}, \tag{31}$$

where

$$r = 2q\rho^2, \quad s = 1 + (q^2-1)\rho^2. \tag{32}$$

The Fano parameters q and ρ^2 are expressed through r and s by the equations

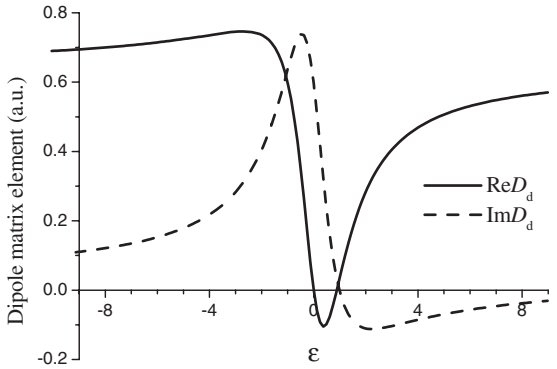

FIG. 3. The real and imaginary parts of the $2p \to Ed$ transition amplitude of Ne atom calculated in the RPAE approximation in the region of the $2s \to 3p$ autoionization resonance.

$$\rho^2 = \frac{1}{2}\left[(1-s) + \sqrt{(1-s)^2 + r^2}\right], \quad q = \frac{r}{2\rho^2}. \tag{33}$$

From comparison between Eqs. (28) and (31) follows

$$r = \frac{\sum_\mu 2q_\mu |D_\mu^0|^2}{\sum_\mu |D_\mu^0|^2} = \frac{\sum_\mu 2q_\mu \sigma_\mu^0}{\sum_\mu \sigma_\mu^0}, \quad s = \frac{\sum_\mu (q_\mu^2 + t_\mu)|D_\mu^0|^2}{\sum_\mu |D_\mu^0|^2}. \tag{34}$$

So, from fitting the numerical RPAE amplitudes by Eqs. (20) we define the parameters a_μ, b_μ, $\mathrm{Re}\, D_\mu^0$, $\mathrm{Im}\, D_\mu^0$, then r and s from Eq. (34), and finally q and ρ^2 from Eq. (33). The parameters q and ρ^2 can be compared with the experimental data where available. It is important to stress that all the equations derived above are applicable not only in the RPAE but in any other approximation taking into account the channel interaction between the resonance and one or several continua.

C. Numerical example

Let us consider in more detail the numerical example of the $3p$ resonance in Ne. Performing calculation in the RPAE with a sufficiently small step in energy near the autoionization resonance we obtain the profile of the resonance numerically. The results of such a calculation for the $2p \to Es$ and $2p \to Ed$ transitions are presented in Fig. 2. From this figure following the description given above we find geometrically the energy and the width of the resonance to be $\omega_0 = 1.822584$ a.u., $\gamma = 0.000835$ a.u. $= 0.023$ eV. After that we fit the $\mathrm{Re}\, D_\mu$ and $\mathrm{Im}\, D_\mu$ shown in Fig. 3 by Eqs. (20), and define from Eq. (26) $q_s = 0.46$, $q_d = -0.93$. In the particular case of the $2p \to Ed$ transition the Argand plot goes very close to the origin. To a good approximation we can accept that both $\mathrm{Re}\, D_d$ and $\mathrm{Im}\, D_d$ appear to be equal to zero at the same energy [see Figs. 2(a) and 3]. It means that the partial cross section at some energy point goes to zero. That leads to substantial simplifications. According to Eq. (24) the cross section can go to zero only provided $t_\mu = 0$. Then the cross section takes the usual Fano form though with the "partial" parameter q_μ

$$\sigma_\mu = \sigma_\mu^0(\omega)\frac{(q_\mu+\varepsilon)^2}{1+\varepsilon^2}. \tag{35}$$

From the condition $t_\mu=0$ and Eq. (27) it follows that $C_{2\mu}=-1$, and the amplitude (17) becomes

$$D_\mu = D_\mu^0\frac{\varepsilon+q_\mu}{\varepsilon+i}. \tag{36}$$

Equations (36) and (35) are also valid for ionization of ns shells when there is only one open channel $ns\rightarrow Ep$.

As a final step we determine from Eqs. (33) and (34) $q=-0.97$, and $\rho^2=0.87$. These numbers are only in a qualitative agreement with the corresponding experimental values for the $3p$ resonance of Ne, $\gamma=0.013(\pm0.002)$ eV, $q=-1.6(\pm0.2)$, and $\rho^2=0.70(\pm0.07)$ obtained in Ref. [28]. On the other hand, it is well known that the RPAE approximation is not sufficient for a correct description of the autoionization resonances in rare gases due to a great contribution of the two-electron excitations which are not taken into account in the RPAE. For a more accurate calculations beyond the RPAE approximation see Refs. [13,14], and references therein.

If a resonance is broad and D_μ^0 (or σ_a and σ_b) and q are not constant within the resonance, Eqs. (20), (24), (28), (29) still remain valid but the Argand plot will deviate from a circle. An example of such a deformed circle for the $6s6p^2(^2D)$ autoionization resonance in Tl atom was presented in Fig. 16 of Ref. [24].

IV. GIANT DIPOLE RESONANCES

Let us turn now to the dipole amplitudes outside the autoionization resonances. For a full characterization of the dipole amplitudes we will include into its definition also the phase shift. Indeed, the angular asymmetry parameter β, the spin polarization parameters [24], and many other characteristics of the photoionization process depend on the phase shifts of the partial waves. The photoelectron wave function $\psi_{\mathbf{p}}^-(\mathbf{r})$ with $\mathbf{p}$ being the photoelectron momentum $E=p^2/2$, in the asymptotic region of large r contains a superposition of a plane wave propagating in the direction of the electron momentum $\mathbf{p}$, and a converging spherical wave, and is commonly presented in the form [26]

$$\psi_{\mathbf{p}}^-(\mathbf{r}) = \frac{1}{\sqrt{p}}\sum_{l,m}(i)^l\exp(-i\delta_l)Y_{lm}^*(\hat{\mathbf{p}})\varphi_{lm}(\mathbf{r}), \tag{37}$$

where

$$\varphi_{lm}(\mathbf{r}) = R_{El}(r)Y_{lm}(\vartheta,\varphi). \tag{38}$$

According to the definition (4) we included into the dipole matrix element only the radial function $R_{El}(r)$ while the phase shift δ_l is factored out. When many-electron correlations are taken into account, for example, in the RPAE approximation, the dipole matrix elements become complex values. They can be presented in the exponential form

$$D_l^{\mathrm{RPAE}} = |D_l^{\mathrm{RPAE}}|\exp(i\Delta\delta_l^{\mathrm{RPAE}}). \tag{39}$$

The phase $\Delta\delta_l^{\mathrm{RPAE}}$ must be added to the phase obtained in the HF approximation. Now we would like to include into a definition such as Eq. (39) also the phase shift from the single particle approximation. But there is an inconvenience in such a definition since the Hartree-Fock phase contains the Coulomb part

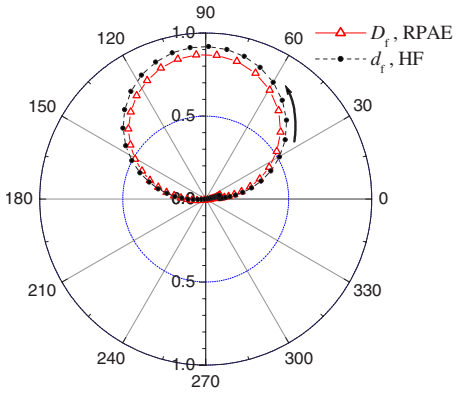

FIG. 4. (Color online) The Argand plot of the $4d\rightarrow Ef$ transition amplitude (in polar coordinates) of Xe atom calculated in the HF and RPAE approximations in the region of the giant dipole resonance $0<E<7$ a.u.

$$\sigma_l = \arg\Gamma(l+1-i/p) \tag{40}$$

which diverges when $p\rightarrow 0$. Therefore we introduce a short range phase τ_l according to the definition

$$\tau_l = \delta_l - \sigma_l. \tag{41}$$

It is implied here that the full phase shift δ_l contains both the Hartree-Fock part, and the part appearing as a result of inclusion of many-electron correlations, for example, in the RPAE ($\Delta\delta_l^{\mathrm{RPAE}}$) or in any other approximation. So, instead of Eq. (39) we shall discuss in the following the dipole amplitudes defined by the equation

$$D_l = |D_l|\exp(i\tau_l). \tag{42}$$

This definition is equally applicable for all photoelectron energies and in all approximations.

Consider now the dipole amplitude $D_f(\omega)$ defined according to Eq. (42) which describes the famous giant dipole resonance in the $4d\rightarrow Ef$ transition in Xe [26,27]. The Argand plot of this amplitude in polar coordinates in the HF and RPAE approximations is presented in Fig. 4. With increasing photoelectron energy E both amplitudes move counterclockwise along the trajectories which are nearly perfect circles. The position of the circle in the complex plane is the same as in the case of the Breit-Wigner amplitude shown in Fig. 1, that is the circle goes through the origin and its center lies on the imaginary axis. Within the resonance the phase to a good approximation is increasing from 0 to π. Therefore we can say that the $4d\rightarrow Ef$ amplitude near the ionization threshold is fully defined by the resonance. This resonance exists already in the HF approximation and therefore is produced essentially by the self-consistent field of the atomic electrons. The many-electron correlations beyond the HF approximation only slightly reduce the magnitude of the dipole amplitude. As to the analytical description, the Breit-Wigner equation (1) can only qualitatively reproduce the behavior of

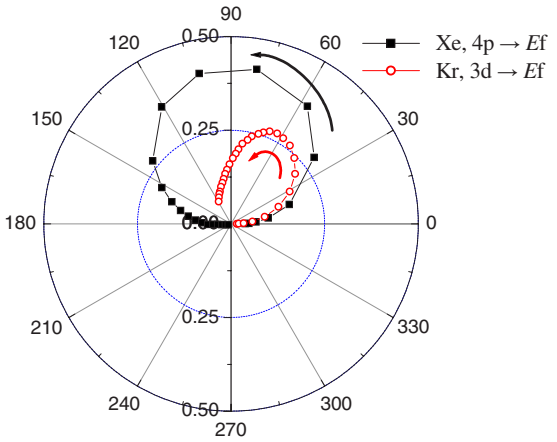

FIG. 5. (Color online) The Argand plot of the $4p \rightarrow Ef$ quadrupole transition amplitude (in polar coordinates) of Xe atom, and of the $3d \rightarrow Ef$ dipole transition amplitude of Kr atom in the HF approximation in the regions of their maxima near the corresponding ionization thresholds.

this amplitude. Much more reliable is the formula proposed by Connerade in Ref. [29].

The resonance behavior of the dipole amplitude $4d \rightarrow Ef$ in Xe is not unique. It was shown in Ref. [30] that all dipole and quadrupole transitions to the Ef final states from all np and nd shells of Xe starting from the $3p$ shell have the resonance behavior, and even the $4s \rightarrow Ef$ octupole transition has it. All these amplitudes produce a circle as an Argand plot, with the phases increasing from 0 to π. It means that there is the resonance of the Breit-Wigner type in every Ef transition in Xe. One example of the quadrupole $4p \rightarrow Ef$ amplitude is shown in Fig. 5.

These results support the explanation [31–33] according to which the f electron in Xe is moving in the double-well potential created by the centrifugal barrier. In the HF approximation we could not check this fact directly due to the nonlocal character of the exchange potential. According to the calculations of Ref. [31,32] with a model Herman-Skillman local potential at low energies the f wave function is pushed out of the atom by the centrifugal barrier, and is concentrated in the outer valley. At the resonance energy the wave function penetrates into the inner valley where the overlap with the bound state wave function strongly increases, and the corresponding matrix element acquires a maximum. At higher energies the amplitude of the wave function goes down, which leads, together with the shift of the first node to a smaller distance, to a decrease of the matrix element.

This general explanation must be equally valid in the HF and in the RPAE approximations as it follows from the direct comparison of the corresponding amplitudes shown in Fig. 4. Therefore one can conclude that the resonance structure of the matrix elements containing the Ef partial wave is a consequence of the double-well shape of the effective potential for the $l=3$ partial wave in the field of the Xe^+ ion. This resonance can be considered as a quasibound state in continuum which with increasing of the nuclear charge Z in Cs, Ba, and La, shifts to smaller energies [34], and is becoming finally the $4f$ bound state at $Z=58$ [34].

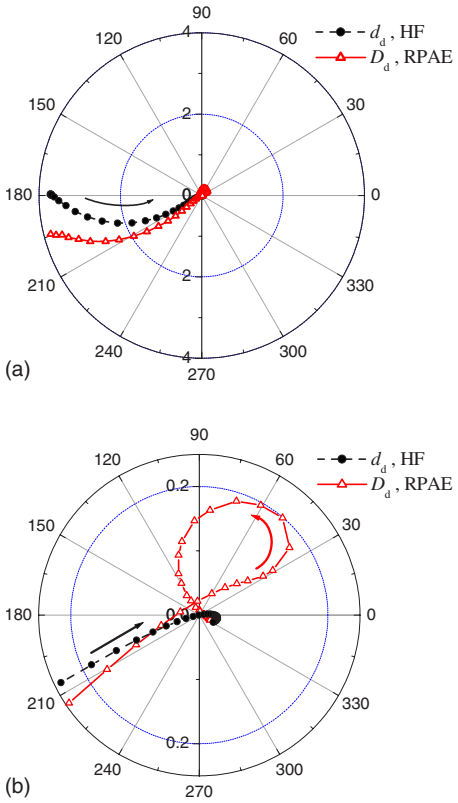

FIG. 6. (Color online) The Argand plot of the $5p \rightarrow Ed$ dipole transition amplitude of Xe atom (in polar coordinates) calculated in the HF and RPAE approximations in the region from the ionization threshold ($E=0$) up to $E=7$ a.u. (a), and in the region $1<E<7$ a.u. (b).

The situation is similar in all atoms around Xe. It is of interest to analyze in the same way the well known maximum in the photoionization cross section of the $3d$ shell of Kr [27]. In Fig. 5 we show the Argand plot of the $3d \rightarrow Ef$ dipole amplitude in Kr. The curve has a form of a loop, and with increasing energy the amplitude moves about it in the counterclockwise direction as it should be in the resonance. Though the phase in the resonance is increasing it remains substantially smaller than π and only slightly exceeds the value $\pi/2$ necessary for recognizing the maximum as a resonance according to the standard definition [35]. The shape of the trajectory deviates from a circle. One can say that this is the border case between the resonant and the nonresonant situation.

V. CORRELATIONAL RESONANCES

Consider now the dipole $5p \rightarrow Ed$ transition in Xe where there is no giant resonance. The Argand plot of this amplitude is shown in Fig. 6(a). Both in the HF and in the RPAE approximations with increasing photon energy the amplitudes sharply decrease in magnitude with a slow variation of the phase. It is well known from the RPAE calculations [27,36,37] that in the region of the $4d \rightarrow Ef$ giant resonance the $5p \rightarrow Ed$ transition also acquires a maximum due to many-electron correlations, that is due to continuum-

continuum interaction between the $5p \rightarrow Ed$ and $4d \rightarrow Ef$ channels. The corresponding Argand plot at higher energies including the giant dipole resonance is shown in Fig. 6(b). The amplitude in this figure is one order of magnitude smaller than in Fig. 6(a). While in the HF approximation the amplitude goes through zero (the Cooper minimum [38]) and at higher energies remains rather small, in the RPAE approximation a loop appears. With increasing photon energy the amplitude moves counterclockwise along the loop. The position of the amplitude maximum corresponds to the cross section maximum in the giant dipole resonance. The trajectory of the amplitude can be interpreted as a resonance superimposed on a background [3]. Due to the presence of the background the trajectory does not go through the origin, and as a consequence the phase shift is increasing less than by π in the resonance. Since the resonance is rather broad the nonresonant contribution is not constant within the width. Moreover, due to the presence of the Cooper minimum in this region the HF amplitude strongly varies as a function of energy. That leads to deviation of the shape of the Argand plot from a circle. The appearance of a loop is a typical manifestation of the correlationally induced resonance in the Argand diagram. Similar behavior we found also in the $5s \rightarrow Ep$ channel near the $4d$ giant dipole resonance of Xe.

VI. MOLECULAR AMPLITUDES

Let us consider now the behavior of molecular dipole amplitudes in the σ^* shape resonances which appear at about 9 eV above the ionization thresholds of K shells of diatomic molecules such as CO and N_2 [39]. Our calculations have been performed in the relaxed core HF (RCHF) and in the random phase (RPA) approximations described in detail earlier in Refs. [40–42].

The photoelectron wave function in the case of molecular photoionization is presented by the partial wave expansion similar to Eq. (37)

$$\psi_{\mathbf{p}}^{-}(\mathbf{r}) = \sum_{l,\lambda} F_{El\lambda}(\mathbf{r})(i)^l \exp(-i\sigma_l) Y_{l\lambda}^*(\hat{\mathbf{p}}). \tag{43}$$

The function $F_{El\lambda}(\mathbf{r})$ is normalized to the energy δ-function and contains only the short-range phase shift (41) while the Coulomb phase shift σ_l according to Eq. (43) is factored out from it. Then the dipole amplitude is defined from the equation

$$d_{l\lambda} = \langle \Psi_{\Lambda_i} F_{El\lambda}(\mathbf{r}) | \hat{d}_\lambda | \Psi_0 \rangle, \tag{44}$$

where $\hat{d}_\lambda = \sqrt{4\pi/3} Y_{1\lambda}(\vartheta, \varphi)$ is the dipole operator, Ψ_0 and Ψ_{Λ_i} are the wave functions of the initial and the final molecular ion state, respectively. We implied here from the very beginning that the σ molecular shell is ionized, therefore the projection of the orbital angular momentum λ in the dipole operator and in the photoelectron wave function coincide. The photoionization cross section is

$$\sigma_{\Lambda_i}(\omega) = \frac{8\pi^2 \alpha \omega}{3} \sum_l (d_{l\sigma}^2 + 2 d_{l\pi}^2). \tag{45}$$

Since in molecules the orbital angular momentum l is not a good quantum number, the dipole selection rules do not restrict the summation over l in Eq. (45). However the partial wave expansion is converging and, for example, at photoelectron energies $E < 3$ a.u. it is sufficient to restrict the summation in Eq. (45) by $0 \leqslant l \leqslant 5$ [19].

In Fig. 7 we show the dipole amplitudes in the complex plane for all dipole allowed $\sigma \rightarrow \sigma$ transitions with $0 \leqslant l \leqslant 5$ from the $1\sigma_g$ [Figs. 7(a)–7(c)] and $1\sigma_u$ [Figs. 7(d)–7(f)] shells of N_2 molecule in the σ^* shape resonance. It is well known [43] that the σ^* shape resonance reveal itself only in the σ channels, therefore we do not show here the amplitudes for the $\sigma \rightarrow \pi$ transitions. The calculations have been performed in the relaxed core HF approximation (RCHF) with a fractional charge (see Ref. [42] for a description of this method). Since the two K shells of N_2, $1\sigma_g$ and $1\sigma_u$, are very closely spaced (the energy splitting is equal to 0.1 eV), many-electron correlations are giving an important contribution [44]. Therefore in Fig. 7 we show both the results of the single particle RCHF calculation with the fractional charge 0.7 [denoted as RCHF(0.7)], and with correlations taken into account in the RPA approximation using the RCHF(0.7) basis set wave functions. The dipole amplitudes presented in this paper are based on the calculations published in Ref. [45].

Let us begin with the discussion of the $1\sigma_g \rightarrow Ef\sigma_u$ transition in N_2. It was shown already long ago by Dehmer and Dill [43] that the σ^* shape resonances in molecules reveal themselves mainly in the $l=3$ partial wave. Indeed, we see that the trajectory of the $f\sigma$ amplitude is rather close to a circle as in the case of the giant dipole resonance in the $4d \rightarrow Ef$ transition of Xe (compare with Fig. 4). Since the $1\sigma_g \rightarrow Ef\sigma_u$ transition gives the main contribution to the cross section, the influence of many-electron correlations on this transition is small, and the RCHF(0.7) and RPA(0.7) results are rather close to each other. At $E=0$ the phase of the amplitude is close to 0, and with increasing energy it tends to π as it should be in the resonance. A similar resonance behavior is displayed also by the $l=5$ partial amplitude both in the RCHF(0.7) and in the RPA(0.7) approximations, though at high energies the trajectory deviates from a circle. The magnitude of this transition is too small to give a noticeable contribution, and this transition was not considered in Ref. [43].

More complicated is the behavior of the $1\sigma_g \rightarrow Ep\sigma_u$ amplitude. In the RCHF(0.7) approximation there is a loop which, by analogy with the atomic cases [see Fig. 6(b)] can be interpreted as a resonance superimposed on the background [3,5]. Actually the amplitude, as well as the corresponding partial cross section, does not have a well defined maximum. In the RPA(0.7) approximation the trajectory changes substantially, and half of a circle appears on it with the counterclockwise motion about it which can be interpreted as a correlational resonance caused by the interaction between the $1\sigma_g \rightarrow Ep\sigma_u$ and $1\sigma_g \rightarrow Ef\sigma_u$ transitions (which is frequently called as l mixing) [5]. The position of the

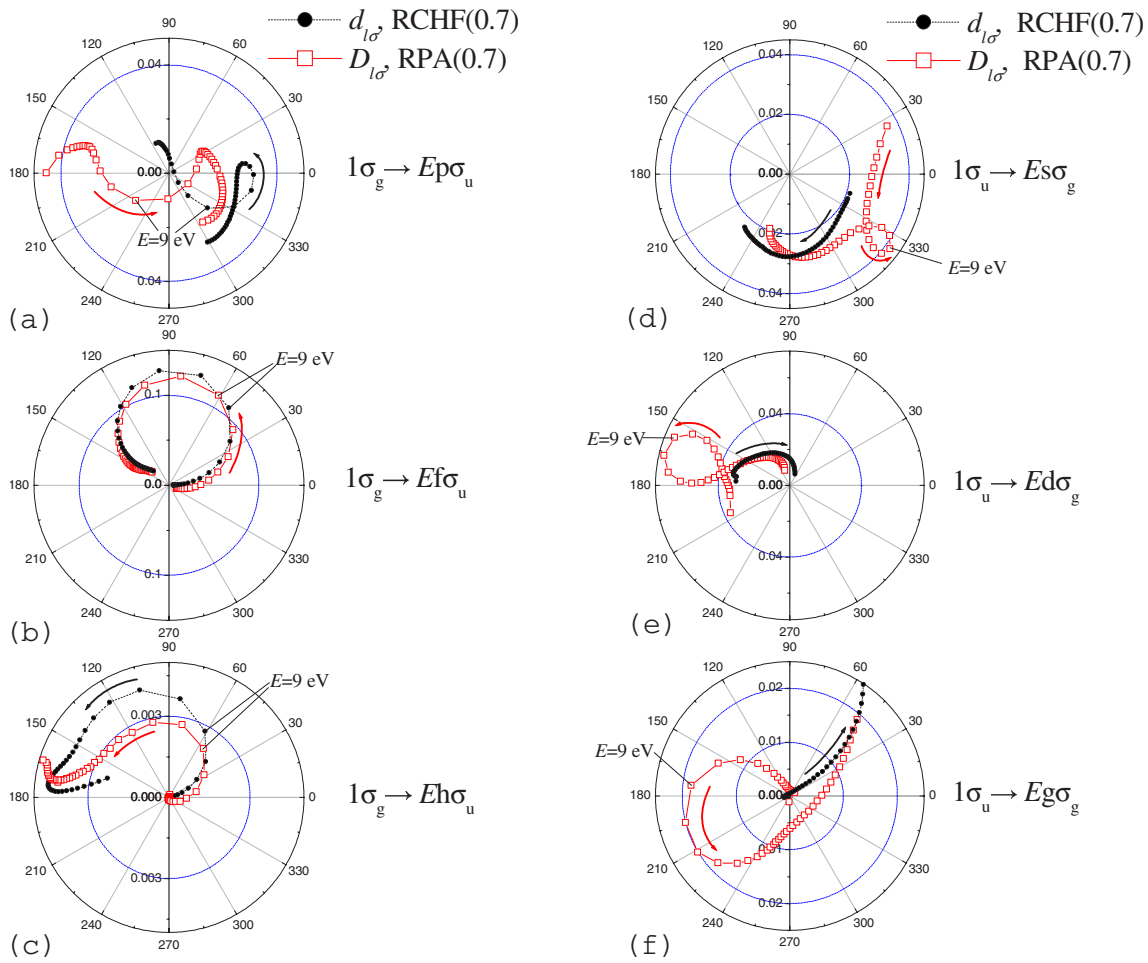

FIG. 7. (Color online) The amplitudes of the $1\sigma_g \rightarrow El\sigma_u$ [(a)–(c)] and $1\sigma_u \rightarrow El\sigma_g$ [(d)–(f)] transitions ($0 \leqslant l \leqslant 5$) of the N_2 molecule in the complex plane (in polar coordinates) calculated in the RCHF(0.7) and RPA(0.7) approximations.

maximum of the σ^* shape resonance at 9 eV photoelectron energy is marked on all trajectories. At this energy the RPA(0.7) amplitude of the $1\sigma_g \rightarrow Ep\sigma_u$ transition has not a maximum but a minimum, and the resonance behavior is reflected only in the shape of the trajectory. One can say that the resonance behavior is revealed in all three transitions from the $1\sigma_g$ shell of N_2 molecule studied here even though the main contribution to the cross section in the σ^* shape resonance, in accord with Ref. [43], is given by the $f\sigma$ partial wave.

In Figs. 7(d)–7(f) we show the dipole allowed transitions from the $1\sigma_u$ shell of N_2. In the single particle RCHF(0.7) approximation all three amplitudes do not show the resonance behavior. This agrees with the conclusion of Dehmer and Dill [43] based on a simple multiple scattering calculation according to which the σ^* shape resonance appears only in the ionization of the $1\sigma_g$ shell. But more advanced calculation with many-electron correlations taken into account in the RPA [44] revealed that due to the intershell correlations between the $1\sigma_g$ and $1\sigma_u$ shells a part of the σ^* shape resonance intensity from the $1\sigma_g \rightarrow El\sigma_u$ channels is transferred into the $1\sigma_u \rightarrow El\sigma_g$ channels. As a result, the partial cross section of the $1\sigma_u$ shell in the RPA(0.7) approximation acquires a maximum, though of lower magnitude than in the $1\sigma_g$ shell. Indeed, as we see from Figs. 7(d)–7(f), every amplitude in the RPA(0.7) approximation acquires a loop which is interpreted as a correlational resonance superimposed on the background. The maximum of each amplitude is placed near the maximum of the σ^* shape resonance at $E=9$ eV photoelectron energy as is marked in all trajectories. That leads to a maximum in the partial cross section of the $1\sigma_u$ shell. The existence of this maximum is now proved experimentally [45]. Summarizing the results presented in Fig. 7 we can say that the σ^* shape resonance reveals itself in that or another way in every partial amplitude calculated in the RPA(0.7) approximation.

VII. SUMMARY

We demonstrated that every resonance in the photoionization amplitude reveals itself in the Argand plot as a circle with the counterclockwise rotation about it when the photon energy is increasing. The most perfect illustration of this behavior is given by the atomic autoionization resonances. From the graphical presentation of the amplitude one can easily connect the parameters of the circle with the energy and the width of the autoionization resonance. We proposed the parametrization for every partial amplitude with a given l

by introducing the equation similar to the Fano equation with the "partial" profile parameter q_μ.

The giant dipole resonances in atoms, as well as the σ^* shape resonances in molecules, reveal themselves basically in the $l=3$ partial wave. Again the corresponding amplitude in the complex plane corresponds to a circle with the counterclockwise rotation about it with increasing photon energy. At zero photoelectron energy the circle starts from the proximity of the origin and the phase in the resonance to a good approximation is increasing by π. This behavior corresponds to a pure resonance without a background. The fact that the giant dipole resonances in atoms and the σ^* shape resonances in molecules reveal themselves in the $l=3$ partial wave is remarkable. These resonances exist already in the HF approximation, therefore they could not be considered as resulting from the many-electron correlations. This is rather a property of the residual ion single particle potential in the field of which the photoelectron is moving.

The other kind of the resonance behavior corresponds to a loop in the Argand plot of the photoionization amplitude. The example of the $5p \rightarrow Ed$ amplitude in the region of the giant dipole resonance in Xe clearly demonstrates that this behavior corresponds to a resonance superimposed on the continuous background. The same conclusion follows also from the analysis of the $1\sigma_u \rightarrow \varepsilon l \sigma_g$ amplitudes with $l=0,2,4$ in N_2 molecule describing the correlational resonance resulting from the channel interaction mainly with the $1\sigma_g \rightarrow \varepsilon f \sigma_u$ transition in the σ^* shape resonance.

The analysis of trajectories of the photoionization amplitudes in the complex plane reveals a new dimension in the photoionization studies. Namely, it allows visualizing every resonance even when the resonance does not reveal itself as a maximum in the partial cross section. For this reason it is very instructive to present the complex photoionization amplitudes as an Argand plot. The possibility to use this kind of information in the complete experiment will be discussed elsewhere while the first step in this direction has been done already in Ref. [19].

ACKNOWLEDGMENTS

The authors thank V. K. Ivanov and N. M. Kabachnik for helpful discussions. This work was supported by the INTAS Grant No. 03-51-4706, and by the DFG-RFBR Grant No. 03-02-04015.

[1] G. Breit and E. Wigner, Phys. Rev. **49**, 519 (1936).
[2] L. D. Landau and E. M. Lifshitz, *Quantum Mechanics (Non-Relativistic Theory)* (Pergamon, Oxford, 1976).
[3] F. Nichitiu, *Phase Analysis in the Physics of Nuclear Interactions* (Mir, Moscow, 1983) (in Russian).
[4] J. Macek and P. G. Burke, Proc. Phys. Soc. London **92**, 351 (1967).
[5] G. C. Schatz and A. Kuppermann, J. Chem. Phys. **59**, 964 (1973).
[6] P. Baillon and P. J. Litchfield, Nucl. Phys. B **94**, 39 (1975).
[7] U. Fano, Phys. Rev. **124**, 1866 (1961).
[8] U. Fano and J. W. Cooper, Phys. Rev. **137**, A1364 (1965).
[9] B. W. Shore, Rev. Mod. Phys. **39**, 439 (1967).
[10] G. Wendin, J. Phys. B **3**, 455 (1970).
[11] N. M. Kabachnik and I. P. Sazhina, J. Phys. B **9**, 1681 (1976).
[12] A. F. Starace, Phys. Rev. A **16**, 231 (1977).
[13] M. Ya. Amusia and A. S. Kheifets, Phys. Lett. **82A**, 407 (1981).
[14] M. A. Kulov, N. O. Vasetskaya, and V. K. Ivanov, J. Electron Spectrosc. Relat. Phenom. **144-147**, 1219 (2005).
[15] *Complete Scattering Experiments*, edited by U. Becker and A. Crowe (Kluwer Academic, New York, 2001).
[16] B. Schmidtke, M. Drescher, N. A. Cherepkov, and U. Heinzmann, J. Phys. B **33**, 2451 (2000).
[17] P. Bolognesi, A. De Fanis, M. Coreno, and L. Avaldi, Phys. Rev. A **70**, 022701 (2004).
[18] N. A. Cherepkov, J. Electron Spectrosc. Relat. Phenom. **144-147**, 1197 (2005).
[19] N. A. Cherepkov, G. Raseev, J. Adachi, Y. Hikosaka, K. Ito, S. Motoki, M. Sano, K. Soejima, and A. Yagishita, J. Phys. B **33**, 4213 (2000).
[20] O. Gessner, Y. Hikosaka, B. Zimmermann, A. Hempelmann, R. R. Lucchese, J. H. D. Eland, P.-M. Guyon, and U. Becker, Phys. Rev. Lett. **88**, 193002 (2002).
[21] M. Lebech, J. C. Houver, A. Lafosse, D. Dowek, C. Alcaraz, L. Nahon, and R. R. Lucchese, J. Chem. Phys. **118**, 9653 (2003).
[22] B. Bederson, Comments At. Mol. Phys. **1**, 65 (1969).
[23] J. Kessler, Comments At. Mol. Phys. **10**, 47 (1981).
[24] N. A. Cherepkov, Adv. At. Mol. Phys. **19**, 395 (1983).
[25] A. N. Grum-Grzhimailo, S. Fritzsche, P. O'Keeffe, and M. Meier, J. Phys. B **38**, 2545 (2005).
[26] A. F. Starace, in: *Handbuch der Physik*, edited by W. Mehlhorn (Springer Verlag, Berlin, 1982), Vol. 31, p. 1.
[27] M. Ya. Amusia and N. A. Cherepkov, Case Stud. At. Phys. **5**, 47 (1975).
[28] K. Codling, R. P. Madden, and D. L. Ederer, Phys. Rev. **155**, 26 (1967).
[29] J. P. Connerade, J. Phys. B **17**, L165 (1984).
[30] N. A. Cherepkov and S. K. Semenov, J. Phys. B **34**, L495 (2001).
[31] J. W. Cooper, Phys. Rev. Lett. **13**, 762 (1964).
[32] S. T. Manson and J. W. Cooper, Phys. Rev. **165**, 126 (1968).
[33] J. P. Connerade, Contemp. Phys. **19**, 415 (1978).
[34] M. Goeppert-Mayer, Phys. Rev. **60**, 184 (1961).
[35] R. G. Newton, *The Scattering Theory of Waves and Particles* (McGraw-Hill, New York, 1966).
[36] M. Ya. Amusia, and V. K. Ivanov, Phys. Lett. **59A**, 194 (1976).
[37] B. Zimmermann, G. Snell, B. Schmidtke, J. Viefhaus, N. A. Cherepkov, B. Langer, M. Drescher, N. Müller, U. Heinzmann, and U. Becker, Phys. Rev. A **64**, 062501 (2001).
[38] J. W. Cooper, Phys. Rev. **128**, 681 (1962).
[39] M. N. Piancastelli, J. Electron Spectrosc. Relat. Phenom. **100**,

167 (1999).
[40] S. K. Semenov, N. A. Cherepkov, G. H. Fecher, and G. Schönhense, Phys. Rev. A **61**, 032704 (2000).
[41] S. K. Semenov and N. A. Cherepkov, Phys. Rev. A **66**, 022708 (2002).
[42] S. K. Semenov, N. A. Cherepkov, T. Jahnke, and R. Dörner, J. Phys. B **37**, 1331 (2004).
[43] J. L. Dehmer and D. Dill, Phys. Rev. Lett. **35**, 213 (1975).
[44] N. A. Cherepkov, S. K. Semenov, Y. Hikosaka, K. Ito, S. Motoki, and A. Yagishita, Phys. Rev. Lett. **84**, 250 (2000).
[45] S. K. Semenov, N. A. Cherepkov, M. Matsumoto, K. Fujiwara, K. Ueda, E. Kukk, F. Tahara, T. Sunami, H. Yoshida, T. Tanaka, K. Nakagawa, M. Kitajima, H. Tanaka, and A. De Fanis, J. Phys. B **39**, 375 (2006).